Vol. 9 №. 1 Trans. Nonferrous Met. Soc. China Mar. 1999

UPPER-BOUND APPROACH ANALYSIS OF DRIVING POWER OF WHEEL FOR CASTEX①

Cao Furong, Shi Zhiyuan and Wen Jinglin
Department of Metal Forming, School of Materials and Metallurgy, Northeastern University, Shenyang 110006, P. R. China

ABSTRACT CASTEX(Cast Extruding) is a relatively new process in the metal working and a further improvement of the CONFORM(Continuous Extrusion Forming) process with feedstock changing into molten metal instead of granular feedstock or rod. A deformation zone division has been made and a driving power formula of wheel groove has been established by applying the Upper-Bound Theorem to the CASTEX process. It is shown by experiment and calculation that the calculated results are in agreement with the experimental ones.

Key words casting extrusion continuous extrusion upper-bound theorem

1 INTRODUCTION

The conventional extruding technologies mostly utilize the linear movement of chief cylinder in hydraulic pressure crock to push the metal in the extruding container to deform plastically. Essentially the driving direction of metal deformation is all of one dimension and linear. In order to realize continuous production, technology of ingot after ingot extrusion(extrusion without remaining) was invented, but not used widely because of the unstable product quality for most metals and alloys.

In 1972, Green[1] subtly utilized periodically rotating wheel with groove on it as the driving power instead of linear driving power to force the metal to go forward along the wheel groove and through the extrusion die to get product. As long as the feedstock was fed into the entry the product then could be gotten continuously, which was called CONFORM(continuous extrusion forming) method[2-4].

In 1984, Langerweger[5-8] turned the feedstock into liquid metal to integrate the casting and CONFORM technology, which was CASTEX(cast extruding or continuous casting and extruding). CASTEX is a further improvement of the CONFORM process, which uses molten metal as feedstock, and lets the material be solidified and extruded in the same machine. Both CASTEX technology and CONFORM technology are the breakthrough of the conventional extruding processes.

Up to now, there are some experimental simulations and mechanical analysis of CONFORM continuous extrusion process[9-13], but there seems no open report on the driving power analysis of CASTEX continuous extrusion process. In this paper, a theoretical formula is derived by applying Upper-Bound Theorem to the CASTEX process, and it is expected that the calculated result is useful for the design of CONFORM and CASTEX machine and their process parameter analysis.

2 SUPPOSING CONDITIONS AND VELOCITY FIELD OF CASTEX

2.1 Operating mechanism of CASTEX

Fig.1 is the schematic diagram of CASTEX process. Liquid metal at a high temperature is fed into the groove of the rotating wheel water-cooled inside and is crystallized. With the rotation of CASTEX wheel the metal is drived by the friction between the groove wall and metal, as soon as the driving stress reaches the yielding

① Received Feb. 27, 1998; accepted Jun. 12, 1998

stress, the metal is then extruded through the die orifice to get product.

2.2 Division of deformation zones

The CASTEX procedure is divided into four zones: L_0 —Liquid phase zone; L_1 —Primary grip zone; L_2 —Grip zone; L_3 —Conventional extruding zone.

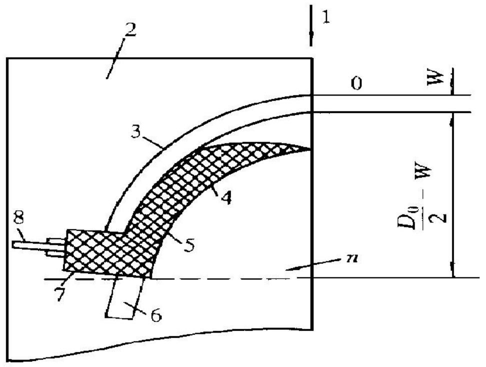

Fig.1 Schematic diagram of CASTEX process
1 —Liquid; 2 —Extrusion shoe;
3 —Seal segment; 4 — Wheel groove;
5 — Metal; 6 —Abutment;
7 — Mini-container; 8 —Product

The practice and calculation all show that the length values of L_1 and L_2 zones are much smaller than the diameter of CASTEX wheel and the length of L_0 zone. So the arcs of L_1 and L_2 zones along the wheel groove can be taken as the quadrates and the x-y-z coordinate is used as shown in Fig.2.

Here the length of L_1 and L_2 is determined by following equations[15]:

$$L_1 = 2W$$

$$L_2 = \begin{cases} n_s W & \text{For radial CASTEX} \\ (n_s - 1) s \cdot W & \text{For tangential CASTEX} \end{cases} \quad (1)$$

$$n_s = \sigma_e / \sigma_s \quad (2)$$

To determine n_s exactly, in the mini-container we should consider the effect of friction between the metal and non-deformation zone in the mini-container on the base of B. Avitzur's solution $\sigma_e/\sigma_s |_{B,A}$ about the plastic deformation and die land.

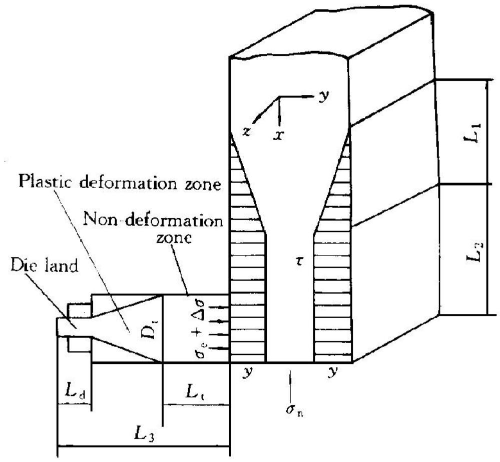

Fig.2 Division of deformation zone and schematic diagram of contact friction stress and normal stress

The increment of extrusion force by friction from the wall of container satisfies the following equation:

$$\Delta\sigma \frac{\pi}{4} D_t^2 = \frac{\sigma_s}{2} \pi D_t L_t \quad (3)$$

$$\Delta\sigma / \sigma_s = 2 \frac{L_t}{D_t}$$

So we get as the follows from Eq.(2):

$$n_s = \sigma_e / \sigma_s = \frac{\sigma_e}{\sigma_s}\Big|_{B,A} + \frac{\Delta\sigma}{\sigma_s}$$

$$= 2 f(\alpha) \ln \frac{D_t}{d} + \frac{2}{\sqrt{3}} \left[\frac{2}{\sin^2\alpha} - \cot\alpha + m\cos\alpha \ln \frac{D_t}{d} + m \frac{L_d}{d} \right] + 2 \frac{L_t}{D_t} \quad (4)$$

where $\Delta\sigma$ is the extruding stress increment imposing on the entry of the mini-container by the friction of container wall, D_t is the diameter of mini-container, L_t is the length of non-deformation zone in the mini-container, σ_s is yielding stress, d is the diameter of the product, L_d is the length of die land of extrusion die, m is friction factor, $f(\alpha)$ is the function of die angle α.

Besides the determination of the length in different deformation zones, the frictional shear stress k and normal stress σ_n on the contact surface between the abutment and metal in the groove are given in Fig.2.

2.3 Supposing conditions and velocity field

2.3.1 Supposing conditions

(1) The metal in L_0 zone is liquid, there is no deformation power.

(2) The arcs of L_1 and L_2 zones along the wheel groove can be taken as the quadrates. Therefore x-y-z coordinate is used.

(3) Divide the L_2 zone into two parts: $L_2 - D_t$ part and D_t part as shown in Fig.3. Suppose there is no relative slide between the metal and the wheel groove in the two parts but slide exists between the abutment and the metal, the inclined plane of abutment and the wheel groove, the mini-container and the metal, the die wall and the metal.

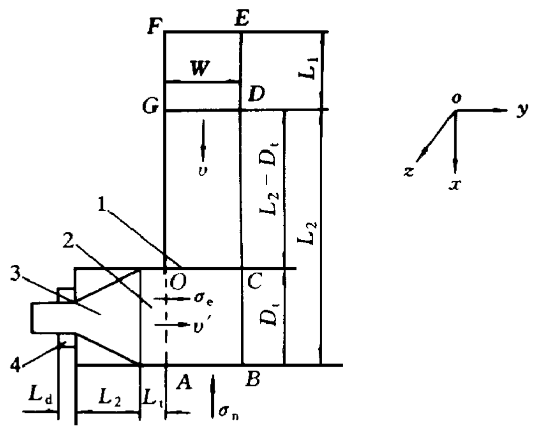

Fig.3 Diagram of determining deformation power in L_2 and L_3 zone

1 —Velocity discontinuous plane;
2 —Nondeformation zone;
3 —Deformation cone; 4 —Die land

2.3.2 Kinematically admissible velocity field

(1) From the supposing conditions, $\varepsilon_i = 0$ in the L_0, L_1 and $L_2 - D_t$ zones.

(2) Kinematically admissible velocity field in D_t zone can be supposed as follows:

$$\left.\begin{aligned} \varepsilon_x &= - v/D_t \\ \varepsilon_y &= v/D_t \\ \varepsilon_z &= 0 \\ \varepsilon_{xy} &= \varepsilon_{yz} = \varepsilon_{zx} = 0 \end{aligned}\right\} \quad (5)$$

The average values of discontinuous velocity variables on OA plane of Fig.3 are approximately as follows:

$$|\Delta V_{fOA}| = v/2 \quad (6)$$

The velocity in y direction of D_t part in Fig.3 is also variable, which increases gradually to v' at the entry OA of mini-container from 0 on the right side wall of wheel groove as metal moves to the left.

The cross-sectional area of groove is W^2, the velocity of metal in groove is v, and the cross-sectional area of metal flowing-out at section OA is shown in Fig.4 (shadow part). The area of shadow part is

$$A = \frac{\pi}{4} D_t^2 [1 - (\arccos \frac{W}{D_t})/90] + \frac{1}{2} W (D_t^2 - W^2)^{1/2} \quad (7)$$

By volume constancy principle we get,

$$W^2 v = A v'$$

Then,

$$v' = 4 W^2 / \{\pi D_t^2 [1 - (\arccos \frac{W}{D_t})/90] + 2 W (D_t^2 - W^2)^{1/2}\} \cdot v \quad (8)$$

So the velocity difference of metal in y direction of D_t zone is v'. The average of discontinuous velocity variables on OC plane is

$$|\Delta V_{fOC}| = v'/2 \quad (9)$$

where W is the width of wheel groove as shown in Fig.4.

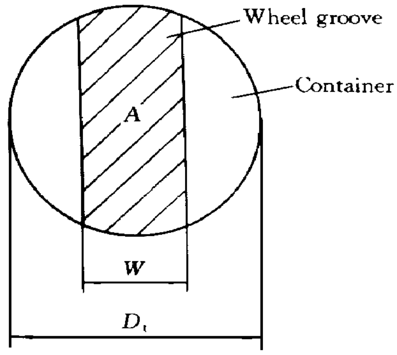

Fig.4 Metal flow area of intercontaction between wheel groove and mini-container

(3) L_3 zone

By applying B. Avitzur's continuous velocity field of spherical coordinate[16] and volume constancy principle, the flowing velocity in the mini-container is obtained as

$$v'' = \frac{4W^2}{\pi D_t^2} v \quad (10)$$

3 DETERMINATION OF UPPER-BOUNDARY POWER OF CASTEX

The Upper-Boundary Theorem of ignoring the power of inertia force, enlarging the power of inner cavities within deformation body and superficial changing power is as follows[16]:

$$W < W^* = \dot{W}_i + \dot{W}_f + \dot{W}_D + \dot{W}_b \quad (11)$$

With Eq.(10) referring to Fig.3 we can determine inner plastic deformation power $\dot{W}_i$, friction loss power $\dot{W}_f$, shear power $\dot{W}_D$ and applied power $\dot{W}_b$ zone by zone. And with zone L_3 we can utilize B. Avitzur's results directly[16].

3.1 Internal plastic deformation power

The general equation for calculating internal plastic deformation is

$$\dot{W}_i = \sum_{j=1}^{3} \dot{W}_{ij} = \sum_{j=1}^{3} \sigma_s \iiint_{v_j} \dot{\varepsilon}_e \mathrm{d} v_j$$

When $j = 1$

$$\dot{W}_{i1} = 0$$

When $j = 2$

$$\dot{W}_{i2} = \sigma_s \iiint_{v_{L_2-D_t}} \dot{\varepsilon}_e \mathrm{d} v_{L_2-D_t} + \sigma_s \iiint_{v_{D_t}} \frac{2}{\sqrt{3}} \dot{\varepsilon}_x \mathrm{d}x \mathrm{d}y \mathrm{d}z$$

$$= \sigma_s \int_0^{D_t}\int_0^{W}\int_0^{W} \frac{2}{\sqrt{3}} \dot{\varepsilon}_x \mathrm{d}x \mathrm{d}y \mathrm{d}z$$

When $j = 3$

$$\dot{W}_{i3} = \frac{\pi}{2} \sigma_s \lambda v'' f(\alpha) \mathrm{d}(\ln \lambda)$$

Referring to Eq.(5), we get

$$\dot{W}_i = 2\sigma_s v W^2 [\frac{1}{\sqrt{3}} + \frac{f(\alpha)}{d} \ln \lambda] \quad (12)$$

where d is the diameter of products; λ is the extrusion ratio; j is the serial number of zones 1, 2, 3.

3.2 Friction loss power

The general equation for calculating friction loss power is

$$\dot{W}_f = \sum_{j=1}^{3} \dot{W}_{fj} = \sum_{j=1}^{3} \iint_{F_j} \tau_j |\Delta v'_f| \mathrm{d} F_j \quad (13)$$

When $j = 1$, in L_1 zone the velocity of metal relative to abutment is $v/2$, the frictional shear stress along the groove increases from 0 to k. So the average value $\tau_1 = k/2 = \sigma_s/4$. Then

$$\dot{W}_{f1} = \int_0^{L_1}\int_0^{W} \frac{k}{2} \frac{v}{2} \mathrm{d}x \mathrm{d}y = \frac{1}{4} k v L_1 W \quad (14)$$

When $j = 2$, the friction loss power in this zone is very complex and composed of the following seven items.

(1) In $L_2 - D_t$ zone, the friction loss power between the metal and seal segments is

$$\int_0^{L_2-D_t}\int_0^{W} k v \mathrm{d}x \mathrm{d}z = k v (L_2 - D_t) W \quad (15)$$

(2) In $L_2 - D_t$ zone, the friction loss power between the metal and groove walls is

$$2\int_0^{L_2-D_t}\int_0^{W} k \cdot 0 \mathrm{d}x \mathrm{d}z = 0 \quad (16)$$

(3) In D_t zone, considering of Eq.(8) and Fig.3, the velocity of metal relative to groove walls is

$$\sqrt{v^2 + v'^2}/2 \quad (17)$$

The frictional shear force is k, so the friction loss power between the metal and groove walls is

$$2\int_0^{L_2-D_t}\int_0^{W} k \cdot \frac{\sqrt{v^2 + v'^2}}{2} \mathrm{d}x \mathrm{d}y \quad (18)$$

(4) In D_t zone, the friction loss power between the metal and the bottom of groove due to the relative movement is

$$\int_0^{D_t}\int_0^{W} k \cdot v \mathrm{d}x \mathrm{d}z = k v D_t W \quad (19)$$

where v is the relative velocity.

(5) Between the metal and the plane of abutment, the relative velocity is v', the friction loss force is k, so the friction loss power is

$$\int_0^{W}\int_0^{W} k \cdot \frac{v'}{2} \mathrm{d}y \mathrm{d}z = \frac{1}{2} k v' W^2 \quad (20)$$

(6) Between the metal and the incline of abutment (as shown in Fig.5) the friction loss power is

$$\int_0^W\int_0^Z k\cdot v\,\mathrm{d}x\,\mathrm{d}z = kvWZ \qquad (21)$$

(7) In L_2 zone, the friction loss power between the effective contact width of wheel and the flash formed by metal leaking (Fig.5) is

$$2\int_0^{L_2}\int_0^{b} k\cdot v\,\mathrm{d}x\,\mathrm{d}z = 2kvL_2 b \qquad (22)$$

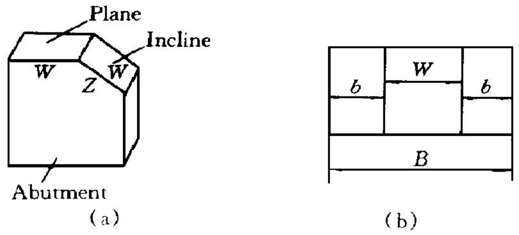

Fig.5 Schematic diagram of contact friction plane between abutment and metal (a) and flash formed by metal leaking between side plane of wheel groove and shoe in L_2 zone (b)

W — Width of wheel groove;

b — Width of flash at one side;

B — Plane incline abutment width of seal segment

From Eqs.(15) ~ (22) we get $\dot{W}_{f2}$ as follows:

$$\dot{W}_{f2} = 2\sigma_s v W^2\{\frac{1}{4}\frac{L_2}{W} + \frac{1}{4}[1+(\frac{v'}{v})^2]^{1/2}\frac{D_t}{W} + \frac{1}{8}\frac{v'}{v} + \frac{1}{4}\frac{Z}{W} + \frac{1}{2}\frac{L_2 b}{W^2}\} \qquad (23)$$

When $j=3$, we get

$$\dot{W}_{f3} = \frac{2}{\sqrt{3}}\sigma_s m\pi\lambda v''(\frac{d}{2})^2\cot\alpha\ln\frac{D_t}{d} + \frac{2}{\sqrt{3}}\sigma_s m\pi\lambda v''\frac{d}{2}L_d + \int_0^{L_t}\int_0^{D_t} k\cdot v''\,\mathrm{d}x\,\mathrm{d}y$$

The last integral item is the frictional power between the metal and the mini-container in nondeformation zone, so the above Eq. becomes

$$\dot{W}_{f3} = 2\sigma_s v W^2[\frac{m}{\sqrt{3}}\cot\alpha\ln\frac{D_t}{d} + \frac{2}{\sqrt{3}}m\frac{L_d}{d} + \frac{L_t}{D_t}] \qquad (24)$$

Putting Eqs.(14), (22) and (23) into (13), we get the whole friction loss power $\dot{W}_f$ as follows:

$$\dot{W}_f = 2\sigma_s v W^2\{\frac{1}{16}\frac{L_1}{W} + \frac{L_2}{4W} + [1+(\frac{v'}{v})^2]^{1/2}\frac{D_t}{4W} + \frac{1}{8}(\frac{v'}{v}) + \frac{1}{4}\frac{Z}{W} + \frac{1}{2}\frac{L_2 b}{W^2} + \frac{m}{\sqrt{3}}\cot\alpha\ln\frac{D_t}{d} + \frac{2}{\sqrt{3}}m\frac{L_d}{d} + \frac{L_t}{D_t}\} \qquad (25)$$

3.3 Shear power on discontinuous velocity plane

The shear power is generally calculated by

$$\dot{W}_D = \sum_{j=1}^{3}\dot{W}_{Dj} = \sum_{j=1}^{3}\iint_{F_j}\tau_j|\Delta v_D|\,\mathrm{d}F_j \qquad (26)$$

When $j=1$

$$\dot{W}_{D1} = 0 \qquad (27)$$

When $j=2$, the shear power on discontinuous velocity plane OC is

$$\dot{W}_{D2} = \int_0^W\int_0^W k\cdot\frac{v'}{2}\,\mathrm{d}y\,\mathrm{d}z \qquad (28)$$

When $j=3$, referring to B. Avitzur's shear power on discontinuous velocity plane, the shear power on discontinuous velocity plane OA is

$$\dot{W}_{D3} = \frac{2}{\sqrt{3}}\sigma_s\pi\lambda v''(\frac{d}{2})^2(\frac{\alpha}{\sin^2\alpha} - \cot\alpha) + \int_0^W\int_0^{D_t} k\cdot\frac{v}{2}\,\mathrm{d}z\,\mathrm{d}x \qquad (29)$$

Using Eqs.(27) ~ (29) in (26), we get

$$\dot{W}_D = 2\sigma_s v W^2[\frac{1}{8}(\frac{v' + vD_t/W}{v}) + \frac{1}{\sqrt{3}}(\frac{\alpha}{\sin^2\alpha} - \cot\alpha)] \qquad (30)$$

3.4 Applied power

The resistance against metal from the abutment is $\sigma_n = (1+n_s)\sigma_s$ [14,15], but as the abutment is static, so the power of abutment to metal is null, i.e.

$$\dot{W}_b = 0 \qquad (31)$$

From Eqs.(11), (12), (25), (30), (31), we get the whole Upper-Bound driving power formula of CASTEX as follows:

$$\dot{W}^* = 2\sigma_s v W^2\{[\frac{f(\alpha)}{d} + \frac{1}{2\sqrt{3}} m\cot\alpha]\ln\lambda + \frac{1}{\sqrt{3}}(1 + \frac{2mL_d}{d} + \frac{\alpha}{\sin^2\alpha} - \cot\alpha) + \frac{1}{16W}[L_1 + 4L_2 + 4(1 + (\frac{v'}{v})^2)^{1/2} D_t + 4Z + \frac{8L_2 b}{W}] + \frac{1}{8}(2\frac{v'}{v} + \frac{D_t}{W}) + \frac{L_t}{D_t}\} \quad (32)$$

Based on Eq.(32), it is easy to determine the driving power of CASTEX wheel. Furthermore, the power of electromotor can be determined by considering the gear ratio, which is helpful for the choosing of electromotor and relevant driving equipment.

It must be pointed out that although the developed power formulae of CASTEX are just about CASTEX of single-groove wheel, they also adapt and fit for the double wheels with one groove for each one or multiple wheels with two or more grooves only considering the number of wheels and grooves in addition[17, 18].

4 EXPERIMENTAL VERIFICATION

The driving power was measured on the self-made CASTEX machine for the producing of Al-Ti-B alloy wires. In the experiment the parameters are as follows:

D_t = 24 mm, d = 9.5 mm, $\alpha = \pi/3$, m = 1, W = 10, L_d = 3 mm, n = 8 r/min, σ_s = 50 MPa at 753 K.

The average yielding stress σ_s = 50 MPa is obtained in following ways: Three holes corresponding to L_0, L_1, L_2 zones were made in seal segment to put thermocouples in each hole to detect the concrete temperature in different zones; one hole was made in extrusion zone L_3 to detect the temperature. The temperature data were obtained by four points temperature detection device. According to the experimental temperature, tensile tests were made on Instron Tensile machine to get yield stresses corresponding to different temperatures. The final yield stress is an average of experiment results.

Using the data above in Eqs.(12), (25), (30), (31) and (32), we get Table 1 for comparison.

Table 1 Comparison of the calculated with the measured

Power	$\dot{W}_i$	$\dot{W}_D$	$\dot{W}_f$	$\dot{W}_b$
Value / kW	0.9785	0.9030	18.546	0
Power	$\dot{W}^*$	$\dot{W}_{exp}$	Error/ %	
Value / kW	/20.428	19.72	13.99	

From Table 1 it can be seen that the error between the calculated and the measured can satisfy the need of engineering. And this error may come from the lowliness of W_i which needs to be further studied.

REFERENCES

1 Green D J. J Inst Met, 1971, 99(2): 76.
2 Pardoe J A. Met Tech, 1984, 11(8): 358.
3 Mitchell K J. Metallurgia, 1982, 49(9): 448 - 451.
4 Gorokhov Y V, Sergcev V M, Gilevich F S *et al*. Tsvetn Met, 1987, (4): 73.
5 Langerweger J and Maddock B. Schweiz Maschinemarkt, 1984, 84(24): 37.
6 Maddock B. Aluminium, 1985, 61(6): 429.
7 Langerweger J and Maddock B. Drahtwelt, 1986, 72 (7 - 8): 174.
8 Langerweger J and Maddock B. Light Met Age, 1988, 46(8): 23.
9 Tirosh J, Grossman G and Gordorn G. Trans ASME: J Eng Ind, 1979, 101(5): 116.
10 Peng D, Yao B Q and Zuo T Y. J Mater Process Technology, 1992, 31(1 - 2): 85.
11 Peng D. J Cent S Univ Technol, 1994, 1(1): 35.
12 Peng Y, Ruan X and Zuo T. J Mater Process Technology, 1994, 45(1 - 4): 539.
13 Etherington C. Wire Industry, 1977, (2): 85.
14 Cao F R, Wen J L and Meng X Y. J Northeastern University, (in Chinese), 1994, 15(4): 368.
15 Cao F R, Wen J L and Zheng X H. Light Met, (in Chinese), 1995, 201(6): 51.
16 Avitzur B. Metal Forming: Processes and Analysis. New York, 1968, 52 - 53, 156 - 163.
17 Hawkes D J and Morgan R E. Light Met Age, 1991, 49(2): 33.
18 Parkinson R D. Wire Industry, 1986, (4): 340.

(Edited by Yuan Saiqian)